International Journal of Biological Macromolecules 121 (2019) 784–795

Contents lists available at ScienceDirect

International Journal of Biological Macromolecules

journal homepage: http://www.elsevier.com/locate/ijbiomac

Biocompatibility, hemocompatibility and antimicrobial properties of xyloglucan-based hydrogel film for wound healing application

Pasquale Picone [a], Maria Antonietta Sabatino [b], Alessia Ajovalasit [b], Daniela Giacomazza [c], Clelia Dispenza [b,c], Marta Di Carlo [a,*]

[a] Istituto di Biomedicina e Immunologia Molecolare (IBIM), Consiglio Nazionale delle Ricerche (CNR), Via U. La Malfa 153, 90146 Palermo, Italy
[b] Dipartimento dell'Innovazione Industriale e Digitale (DIID), Università degli Studi di Palermo, Viale delle Scienze, Edificio 6, 90128 Palermo, Italy
[c] Istituto di Biofisica (IBF), Consiglio Nazionale delle Ricerche (CNR), Via U. La Malfa 153, 90146 Palermo, Italy

ARTICLE INFO

Article history:
Received 13 July 2018
Received in revised form 3 October 2018
Accepted 14 October 2018
Available online 18 October 2018

Keywords:
Wound healing
Biocompatibility
Hemocompatibility
Adhesiveness
Bacterial growth

ABSTRACT

Crosslinked xyloglucan-poly(vinyl alcohol) based hydrogel films are interesting materials for wound healing applications. This work focuses on the hydrolytic degradation and consequent morphological modification of a XG-PVA film and on its interaction with cells, blood, bacteria. Biocompatibility of the film was assessed *in vitro* by investigating different aspects, such as cell viability, oxidative stress level, mitochondrial dysfunction and specific stress biomarkers. Partial adhesiveness was demonstrated by performing different attaching assays and phalloidin staining. Hemocompatibility of XG-PVA film after interaction with blood was evaluated by using a multi-parametric approach, including human Red Blood Cells (RBC) count, hemolytic response and platelets activation. Thrombin and fibrinogen concentrations were examined as marker of the coagulation cascade. After direct contact with human blood and peripheral blood mononuclear cells (PBMC), no evidence of cell defense response was observed. Antimicrobial activity of XG-PVA film was tested against *Escherichia coli* (*E.coli*). XG-PVA film promotes bacterial retentivity and provides mechanical protection against bacterial infiltration. After loading the film with ampicillin, an inhibitory *E. coli* growth zone was observed. All together these results indicate that the XG-PVA system is a promising material to be tested *in vivo* for wound healing applications.

1. Introduction

Wound healing is a natural process that begins when a physical or thermal injury disrupts the epithelial lining of the skin. On the basis of the repairing time, wounds can be classified as acute or chronic [1]. Acute wounds can be due to accident or surgical injury and their healing depends on the area, depth and damage of the different skin layers, and generally occurs in a relatively short time. Chronic wounds can be due to decubitus, leg ulcers or burns. They do not progress through the canonical stages of healing, requiring longer time for their repair.

Wound treatment and therapy represent an economically challenging problem for healthcare systems worldwide, especially for the treatment of chronic wounds. Regeneration of damaged tissue is a dynamic process in which a sequence of integrated cellular and molecular events is necessary to restore homeostasis [2]. The healing process occurs in three different ordered and overlapping stages: inflammation, proliferation and remodeling. During this process, different cellular components participate to the healing, involving the blood coagulation cascade and the immune system together with the extracellular-matrix proteins, cytokines and growth factors [2]. Although for most injuries the wound repair process leads to the restoration of the original tissue architecture, in some cases dysfunction in the organization of fibroblasts cells, large deposition of extracellular matrix components, such as collagen, and alteration of local vascularization can induce scar formation. As mentioned before, time is an important aspect in tissue repair and the research in this field is addressed to the development of new products and therapies that can accelerate wound healing. Suitable wound dressing materials are available for specific wound types, to address the different requirements of the wound healing stages [3,4]. In general, an ideal wound dressing should: a) be sterile; b) be non-cytotoxic to healthy tissues; c) provide mechanical protection; c) promote or maintain a moist wound environment; d) absorb the exudate excess; e) allow gas exchange between damaged tissue and environment; f) be only partially adhesive to the wound, thus allowing its removal without pain or trauma; g) provide protection against bacterial infection or contamination. Modern wound dressings can be composed of either natural polymers, such as chitosan, collagen, hyaluronic acid or alginate, or synthetic polymers including polyvinyl alcohol, polyvinylpyrrolidone and polyurethane, in the form of hydrogels, pastes, films, fibers or foams [5–7]. Furthermore, modern wound dressings often play

* Corresponding author at: Istituto di Biomedicina e Immunologia Molecolare CNR, Via U. La Malfa 153, 90146 Palermo, Italy.
E-mail address: marta.dicarlo@ibim.cnr.it (M. Di Carlo).

https://doi.org/10.1016/j.ijbiomac.2018.10.078
0141-8130/

an active role in wound treatment and management, rather than providing protection only, like the traditional ones. Indeed, they can be combined with bioactive molecules, such as antimicrobials, antibiotics, vitamins, or growth factors that can accelerate the healing process [8–11]. Hydrogels are successfully applied as wound healing materials for their open porous microstructure that allows the incorporation of large amounts of water and good permeability to aqueous solutes, thus resembling most of the living tissues; for their elasticity and flexibility that permit to conform to different body sites [12,13]; and for their relative low costs. Hydrogels can be loaded with anti-inflammatory or antimicrobial agents, incorporate growth factors or stem cells that can promote cell growth, wound healing and skin regeneration [14–17]. Furthermore, the polymeric network forming the hydrogel is a dynamic architecture that can undergo changes in time in response to mechanical, physical and (bio)chemicals cues [18]. Indeed, the network modifications (hence pore size, pore walls hydrophilicity) can be a stimulus for cells biological functions (adhesion, migration, proliferation) and/or, in turn, the contact with living cells secreting various biomolecules can modify hydrogel structure and morphology modifications [19,20]. In a recent paper, we have presented a novel family of hydrogel films based on blends of xyloglucan (XG) and polyvinyl alcohol (PVA) [21].

XG is a hemicellulose that occurs in the primary cell walls of all vascular plants and as storage polysaccharide of different seeds [22]. Here, we have used the Tamarind kernel xyloglucan, characterized by a cellulose-like backbone with branched (1–6)-α-xylose or (1–2)-β–galactoxylose side chains [23–25].

XG was chosen as the main component of this formulation thanks to its low cost, biodegradability, biocompatibility, intrinsic anti-inflammatory properties and its potential beneficial effects for skin regeneration [26–28].

Preliminary tests on the covalently crosslinked film variants demonstrated no cytotoxic effects caused by the release of toxic compounds [21]. These results encouraged us to proceed with further physicochemical evaluations and *in vitro* biological characterizations, in order to validate their use as wound healing materials. In particular, we analyzed the biocompatibility in terms of direct contact effects, oxidative stress and mitochondrial dysfunction, adhesion ability, hemocompatibility, absence of immunogenic response, and antibacterial activity. Furthermore, we investigated the effect of the incorporation of an antibiotic on the film antimicrobial activity.

2. Materials and methods

2.1. XG/PVA film preparation and characterization

Tamarind xyloglucan (XG) was kindly provided by DSP Gokyo Food and Chemical Co. (Japan) with a molar ratio among glucose, xylose and galactose units of 2.8:2.25:1 [29,30].

XG molecular weight, measured by static light scattering measurements and Zimm plot analysis, resulted 1.185 ± 0.085 MDa. [21] Poly (vinyl alcohol) (PVA, MW = 16 kDa, 98% degree of deacetylation) was purchased from Sigma-Aldrich. XG (4% w/v) and PVA (2% w/v) PVA solutions were mixed at 1:1 volume ratio for 30 min, acidified to pH 2.5 (1 M HCl), and added with glutaraldehyde (GA, Sigma Aldrich). The reaction is carried out at low pH in order to increase the reaction rate and favor the formation of acetal bonds. [31]

Stirring was continued for 1 h at room temperature, then NaOH (1 M) was added to increase pH to 7.0. Finally, glycerol (Gro, Sigma Aldrich) was added. The solution was cast into glass moulds and incubated in an environmental chamber at room temperature and 50% relative humidity (RH) to a constant weight.

The amount of water retained by the air-dried film was about 15% wt. To determine the gel fraction (GF) the soluble portions of the film were extracted with MilliQ water at 70 °C until constant weight of the residual material was obtained. [21]. GF resulted 93 ± 4%.

2.2. In vitro hydrolytic degradation

In vitro degradation tests were performed by immersion of dry film samples (five samples per data point from different preparation batches) in PBS (pH 7.4) at 37 °C. At pre-determined time intervals (4, 8, 12 days and 6 weeks), the samples were removed from the degradation medium, washed with distilled water to remove the soluble fractions, freeze-dried and then weighed.

2.3. Fourier transform infrared spectroscopy (FTIR)

FTIR analysis was carried out using a Fourier Transform Infrared Spectrometer (FTIR) (Spectrum Two, Perkin Elmer). Spectra were collected by accumulation of 32 scans between 4000 and 450 cm^{-1}, with a resolution of 4 cm^{-1}. Before the analysis, samples were washed with MilliQ water, lyophilised in the presence of KBr and then compressed into disks.

2.4. Scanning electron microscopy (SEM)

Surface morphology was imaged by a Field Emission Scanning Electron Microscope (FESEM-JEOL) at an accelerating voltage of 10 kV. Samples subjected to *in vitro* degradation were washed with MilliQ water, frozen in liquid nitrogen and freeze-dried. The samples were fractured to expose their inner structure, mounted on aluminium stubs by means of a graphite adhesive layer, and gold coated by JFC-1300 gold coater (JEOL) for 90 s at 30 mA before the analysis.

2.5. Uptake and release of Atto 633 fluorescent probe

Weighed pieces of XG-PVA films were immersed in a Atto 633/PBS solution (1,33 μg/mL) to test their uptake ability. At pre-determined times, an aliquot of Atto 633 solution was collected and analyzed using the UV-670 Spectrophotometer (Jasco). After the measurement, the collected aliquot was returned to the uptake solution. For the release study, the loaded Atto 633 film was immersed in fresh PBS medium and, at predetermined times, an aliquot of the solution was analyzed through UV spectrophotometry and replaced with fresh PBS medium. The concentration of Atto 633 both in the uptake and release solutions was determined by measuring the absorbance at 629 nm.

2.6. Cell culture and treatments

A549 human lung carcinoma epithelial cells were cultured with RPMI 1640 medium (Celbio srl, Milan, Italy) supplemented with 10% fetal bovine serum (FBS) (Gibco-Invitrogen, Milan, Italy), 2 mM glutamine, 1% penicillin and 1% streptomycin (50 mg/mL). Cells were maintained in a humidified 5% CO_2 atmosphere at 37 ± 0.1 °C. For cytocompatibility assays (MTS, ROS and JC-1 assays) and contact test, XG-PVA films with the weight of 5 and 10 mg were sterilized by UV irradiation for 30 min and placed on A549 epithelial cells monolayer (6×10^4 per well) of 96-well flat-bottom culture plate, and incubated for 48 h.

2.7. Determination of cell viability

Cell viability was measured by MTS assay (Promega Italia, S.r.l., Milan, Italy). MTS [3-(4,5-dimethylthiazol-2-yl)-5-(3-carboxymethoxyphenyl)-2-(4-sulphophenyl)-2H-tetrazolium] was utilized according to the manufacturer's instructions. After treatment, 20 μL of the MTS solution were added to each well and the incubation was continued for 1 h at 37 °C in humidified incubator with 5% CO_2. The absorbance was read at 490 nm on the Microplate reader Wallac Victor 2 1420 Multilabel Counter (PerkinElmer, Inc. Monza, Italy). Results were expressed as the percentage of MTS reduction relative to the control. Treated and untreated cultured cells were fixed with 4%

paraformaldehyde and cell morphology and shape was visualized by staining with phalloidin (1:50), a dye interacting with polymeric actin, for 30 min at room temperature (r.t.). Nuclei were visualized by using Hoechst 3342 (5 mg/mL) for 20 min at room temperature. After incubation, samples were washed with PBS and visualized with a fluorescence microscope (Zeiss Axio Scope).

2.8. Analysis of reactive oxygen species (ROS) generation

To assess ROS generation, A549 cells were plated in a 96-well optical bottom white microplate. After incubation with the XG-PVA film, as described above, or with tert-butyl hydroperoxide (TBH) (0.5 mM) as positive control, 1 μM dichloro fluorescein diacetate (DCFH-DA) was added for 10 min at r.t., according to manufacturer's instructions and as described in [32].

2.9. Analysis of mitochondrial activity

Mitochondrial membrane potential was measured using 5,5′,6,6′-Tetrachloro-1,1′,3,3′-tetraethylbenzimidazolyl-carbocyanine iodide (JC-1)-Mitochondrial Membrane Potential assay kit (Molecular Probes, Eugene, OR, USA) according to manufacturer's instructions. Briefly, A549 cells were plated in a 96-well transparent microplate for microscope fluorescence and, after placing the XG-PVA films, were incubated with 2 mM JC-1 fluorescent dye, as described by [33].

2.10. Western blot analysis

Total protein extraction and Western blotting was performed according to [33]. Western blot was incubated with anti-hsp70 (1:1000; Cell signaling), anti-hsp60 (1:1000; Santa Cruz); anti-peroxiredoxin III (1:1000; Sigma) anti β-actin (1:1000; Sigma) antibodies. Primary antibody was detected by Odyssey scanner (L. Licor).

2.11. Evaluation of cell adhesion

For cell adhesion assay, UV sterilized XG-PVA film was placed on the bottom of some wells of a 96-well culture plate. A549 cells were cultured on the XG-PVA film or directly on the cell culture plastic (CCP) at different concentrations (150,000 or 300,000 or 600,000 cells/mL). After 24 h, the unattached cells were removed and transferred in a new cell culture plate, cultured for additional 24 h and submitted to MTS assay. The adhered cells were directly quantified by MTS assay and their morphology was observed by optical microscopy (Leika).

2.12. Blood compatibility and immune response assays

Blood from human volunteer donors (3 mL) was drawn directly into K2-EDTA-coated Vacutainer tubes to prevent coagulation and incubated with XG-PVA films (1 cm^2) for 3 h and mixed by gentle manual inversion. An aliquot of the blood was utilized for cell count and another one for thrombolytic and hemolytic assays. Total White Blood Cells (WBC) number and composition (neutrophils, lymphocytes, monocytes, eosinophils, basophils), Red Blood Cells (RBC) number and parameters (hemoglobin blood concentration (Hgb), Mean Corpuscular Volume (MCV), Mean Corpuscular Hemoglobin (MCH), Mean Corpuscular Hemoglobin Concentration (MCHC), Red Cell Distribution Width (RDW)), platelet number and parameters (mean platelet volume (MPV) and distribution width (PDW) and plateletcrit (PCT)) were measured by a Beckman Z1 Coulter Particle Counter. For thrombolytic assays, the blood was centrifuged at 4000 rpm for 5 min and the plasma collected and analyzed for: prothrombin time (PT) assay, expressed as international normalized ratio (INR); activated partial thromboplastin time assay (aPTT); fibrinogen concentration and antithrombin III assay by using the ACL Laboratory Instrumentation. For hemolysis assays, the blood was centrifuged at 500 rpm for 5 min, and hematocrit and plasma levels were marked on the tube and processed according to [33]. C3 and C4 activation in the plasma was measured by an enzyme-linked immunosorbent assay (ELISA, Abcam).

2.13. Peripheral blood mononuclear cells treatment

Peripheral blood mononuclear cells (PBMCs) were isolated from 5 mL of venous blood collected early in the morning from healthy donors (age range: 20–30 years old) in EDTA (heparin) tubes according to [33]. PBMCs were incubated with XG-PVA film (10 mg) or with lipopolysaccharide (LPS) (0.1 mg/mL) and H_2O_2 (50 μM) for 24 h.

2.14. Antibacterial test

Antimicrobial activity of XG-PVA film was tested on *Escherichia coli* (*E. coli*), a gram-negative bacterium. Depending on the test, bacterial strain was grown in typical Luria-Bertani (LB) broth medium or in LB agar plates. The day before the test, a single colony was inoculated in LB medium and incubated at 37 °C overnight (o.n.). An aliquot (5 μL) of an o.n. bacterial culture was added to two test tubes containing fresh LB medium and left to grow for 120 min. The exponential growth was determined by spectrophotometric measurement at 600 nm (OD_{600}). Then, UV sterilized XG-PVA film (1 cm^2) was added to one of the test tube and the absorbance was measured every 30 min up to 2 h.

2.15. Infiltration and retentivity bacterial tests

E. coli was o.n. cultured in LB medium at 37 °C. 10 μl of the *E. coli* culture were gently dropped in the center of a XG-PVA film surface (about 1 cm^2) placed on LB plate and 10 μL directly on LB plate (control) and incubated at 37 °C o.n. Then, three pieces of agar of about 0.3 cm^2 were taken from the area under the XG-PVA film, only with bacteria, far from the film (control) and incubated in LB medium (experimental procedure is schematically shown in Supporting Information Fig. S1 A). After 2 h, the bacterial growth was determined by spectrophotometric measurement (OD_{600}). For the retentivity test (experimental procedure is schematically shown in Supporting Information Fig. S1 B), 10 μL of a diluted (1:1000) o.n. *E. coli* culture were spread onto LB agar plates in which some pieces of UV sterilized XG-PVA (1 cm^2) film were placed. After o.n. incubation at 37 °C, the film, the agar below the film and the agar far from the film (control) were removed and separately incubated in LB liquid medium for 2 h. UV–vis absorbance was measured at 600 nm (OD_{600}).

2.16. Ampicillin XG-PVA loading and antibacterial activity

Different pieces of XG-PVA film of the same dimensions were soaked with different concentrations (0.5 and 2.5 mg/mL) of ampicillin (Sigma Aldrich) for 2 h. 50 μL of a diluted (1:100) *E. coli* o.n. culture were spread on LB agar plates and after 10 min the ampicillin-loaded XG-PVA samples were placed in the center of the LB agar plates and o.n. incubated at 37 °C. The inhibitory effect on bacteria growth was determined by measuring the diameter of the bacteria-free zone.

2.17. Statistical analysis

Results, in the cell experiments, were expressed as the percentage of MTS reduction relative to the control and presented as the mean ± standard deviation (SD). The significance of the differences in the mean values of multiple groups was evaluated using analysis of variance (ANOVA). Differences were considered significant when the *p*-value was ≤0.05.

3. Results

3.1. In vitro hydrolytic degradation

Xyloglucan/polyvinyl alcohol (XG-PVA) film, were prepared from solutions of XG and PVA, crosslinked by addition of glutaraldehyde. The covalent network is formed involving both XG and PVA chains. Besides, both glutaraldehyde and glycerol, the last one added to the formulation prior to casting and air-drying, can be grafted to the network, increasing the network mesh size and providing high flexibility to the films [21]. The as-prepared film appears homogenous, colorless and slightly opaque. When immersed in water, it becomes white (see Fig. S2 in Supporting Information).

Samples of the film were subjected to *in vitro* hydrolytic degradation in PBS at 37 °C. The weight loss was measured after 4, 8, 20 and 30 days. The hydrogel loses 47 ± 4% of its initial mass after 4 days of incubation; does not show any further significant change of weight during the following 4 days; loses an overall 60 ± 8% of the initial mass after 20 days and 67 ± 9% after 30 days of incubation. In Fig. 1A–D, the SEM micrographs of the as-prepared, 1, 8 and 30 days-degraded films are reported. The as-prepared XG-PVA film showed a fairly uniform microporous structure with an average pore size of *ca.* 20 μm (Fig. 1A). The porosity of the degraded films increased in size (Fig. 1B-D) with time, becoming *ca.* 80 μm after 1 day and 200 μm after 30 days. FTIR measurements have been performed also on the film before and after 30 days of hydrolytic degradation. The spectra are shown as Fig. S3 of Supporting Information. The spectrum of the as-prepared film has been already described elsewhere. [21] The exposure of the film to water at 37 °C causes only small changes in the relative height of the peaks of some functional groups of the network. In particular, we observe the attenuation of the band at 1720 cm^{-1} and the relative increase of the band at 1150 cm^{-1}.

3.2. Uptake and release of Atto 633 fluorescent probe

The ability of the film to absorb and release molecules was spectroscopically tested by using Atto 633 fluorescent hydrophilic dye (Fig. 2). Film specimens, previously swollen in water to their equilibrium state, incorporated *ca.* 80% of the dye present in the uptake solution and released, in 24 h, *ca.* 98% of the loaded amount. The uptake and release of the probe can be modeled as Fickian diffusion. This suggests that the swollen film has interconnected porosity.

3.3. Cytocompatibility of XG-PVA film

In order to test the XG-PVA film cellular cytotoxicity, human A549 epithelial cell lines were utilized as model to measure cell viability after 48 h of incubation. *In vitro* cytotoxicity was evaluated using two different tests, the "direct-contact" method and the MTS cell viability assay. Results were analyzed according to the ISO10993-5 standard guidelines [34]. The direct-contact method is based on the observation of changes in cell morphology and number, when the material is placed in direct contact with cells; the toxicity is scored from 0 to 4, (0 = non-cytotoxic, 1 = slightly cytotoxic, 2 = mildly cytotoxic, 3 = moderately cytotoxic and 4 = severely cytotoxic). Cells around the tested sample showed normal morphology (no toxic response including detachment, lysis, extensive vacuolization, reduction of cell growth) and no change

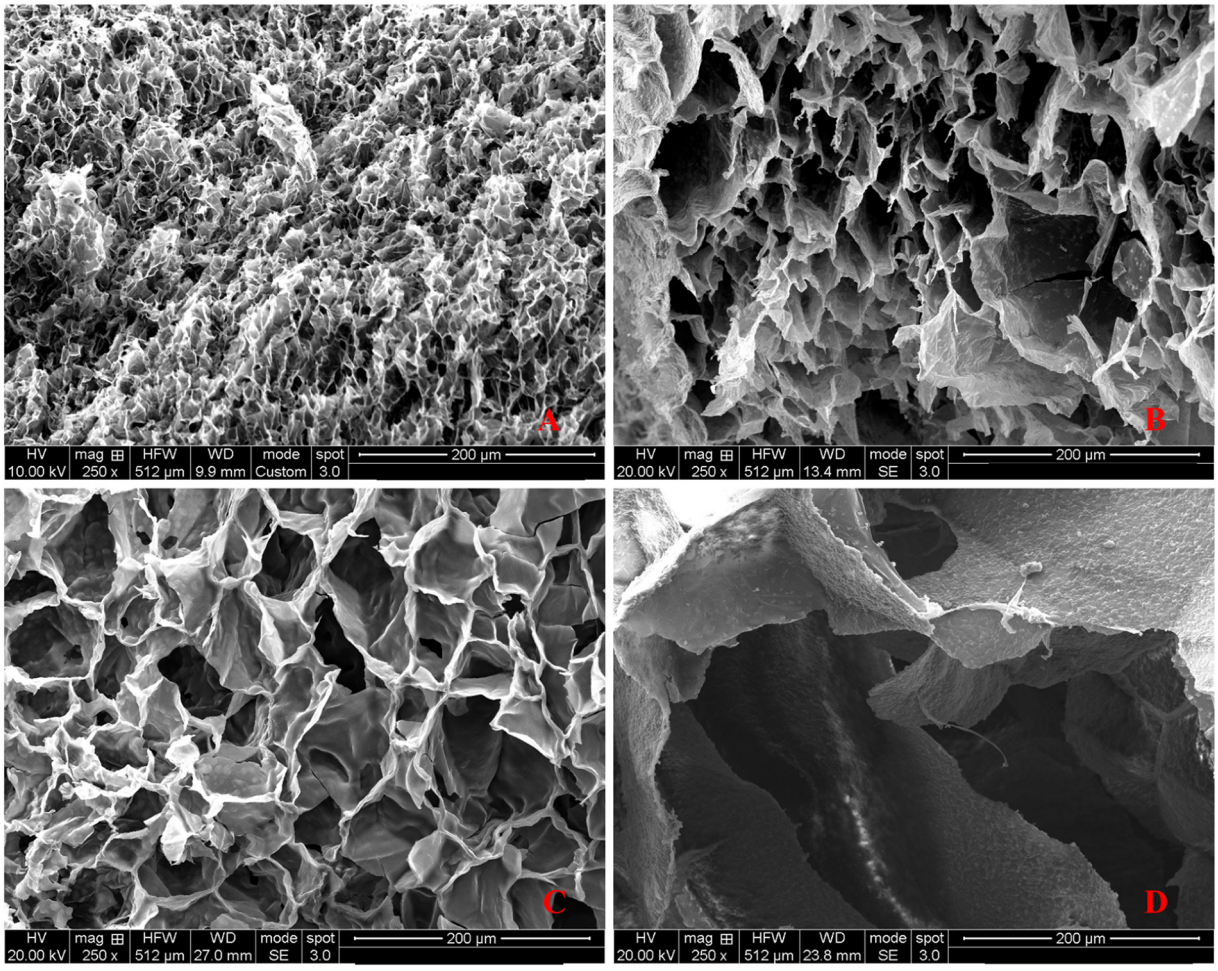

Fig. 1. SEM images of XG/PVA films cross-sections: as-prepared (A); after 1 (B), 8 (C) and 30 (D) days of incubation in PBS at 37 °C.

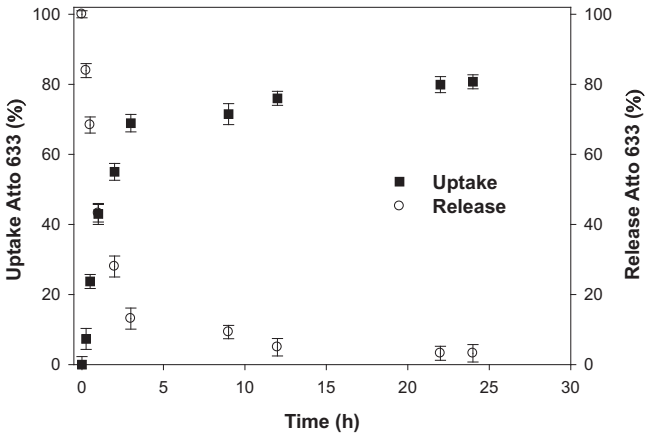

Fig. 2. Uptake/release profiles of Atto 633 by XG-PVA films.

in their number and can be classified of grade 0 [34]. Furthermore, after film removal, the underlying cell layer portion appeared morphologically similar to the uncovered parts of the same layer (Fig. 3A). MTS assay is based on the measure of the mitochondrial metabolic activity and is routinely used as index of cellular viability and proliferation. According to the ISO10993-5 guidelines, a biomaterial is considered cytotoxic when its viability is below 70%. After exposure of A549 epithelial cells to samples of XG-PVA film of two different weights for 48 h, we found *ca.* 90% cell viability for both samples, indicating that the contact with the biomaterial did not induce cell toxicity or abnormal cell growth (Fig. 3B).

3.4. XG-PVA film does not induce cellular stress in A549 cells

Absence of oxidative stress and mitochondrial dysfunction are also considered indicative metabolic parameters of biocompatibility. To evaluate reactive oxidative species (ROS) formation in A549 epithelial cells exposed to XG-PVA film or TBH, used as positive control, a DCF assay was performed. Fluorescence analysis demonstrated that the amount of intracellular ROS was comparable to that expressed at basal level (Fig. 4A). In contrast, increased fluorescence was obtained in TBH treated cells (Fig. 4A). The results were visualized by fluorescence microscopy (Fig. 4B). To detect the presence of mitochondrial membrane depolarization, A549 cells were seeded on top of the sample and subjected to JC-1 assay, in which the red/green fluorescence intensity ratio indicates mitochondrial impairing. In samples exposed to XG-PVA for 48 h, red fluorescence signals, comparable to the control, were detected indicating that the physiological mitochondrial membrane potential was not changed (Fig. 4C). In contrast, in the CCCp treated sample, used as positive control, green fluorescence was higher than red fluorescence (Fig. 4C). Quantification of red/green fluorescence intensity ratio is shown in the histogram of Fig. 4D. Furthermore, the stress response of cells in contact with XG-PVA samples of various sizes and for different contact times was evaluated. The expression of Hsp70, a stress response protein [35,36]; Hsp60, a marker of mitochondrial impairment [37]; and peroxiredoxin III, an antioxidant enzyme [38] was analyzed. After 1 h of incubation (cell-film contact), Hsp70 expression was enhanced in a size-dependent manner, whereas after 3 h returned to the basal levels suggesting that a protective or adaptive response was activated (Fig. 4E–F). In agreement with the results of DCF and JC1 assays, no significant differences in the Hsp60 and peroxiredoxin III expression was detected with respect to the control was detected (Fig. 4E–F).

3.5. Evaluation of cell attachment on XG-PVA film

A549 cells were seeded at three different densities and cultured directly on the cell culture plastic (CCP) containing or not (control) the hydrogel film. After 24 h, the medium containing the unattached cells was removed and transferred into a new cell culture plate to test cell viability after further 24 h (Fig. 5A). Additionally, the attached cells were visualized by microscope inspection and quantified by MTS assay. No significant alteration in the morphology of the attached cells was observed (Fig. 5B). Furthermore, the data summarized in Fig. 5C show that the percentage of cells attached to the film was lower with respect to the control, for all the investigated concentrations of seeded cells, increasing with the seeded cell density. The viability of the unattached cells was detected (data not shown). To ascertain that the attached cells maintained the ability to grow on the XG-PVA film, we chose to analyze the sample seeded at 300.000/mL cellular density that showed about a 40% of adhesion. After culturing for additional 24 h, cells were submitted to MTS assay. The data indicated that cells were able to grow on the film reaching levels comparable to the control (Fig. 5D). Finally, the absence of cellular morphological alterations and fragmented nuclei were confirmed by staining cells cytoskeleton and nuclei with phalloidin and Hoechst 3342, respectively (Fig. 5E). Furthermore, phalloidin staining revealed the presence of focal adhesions and

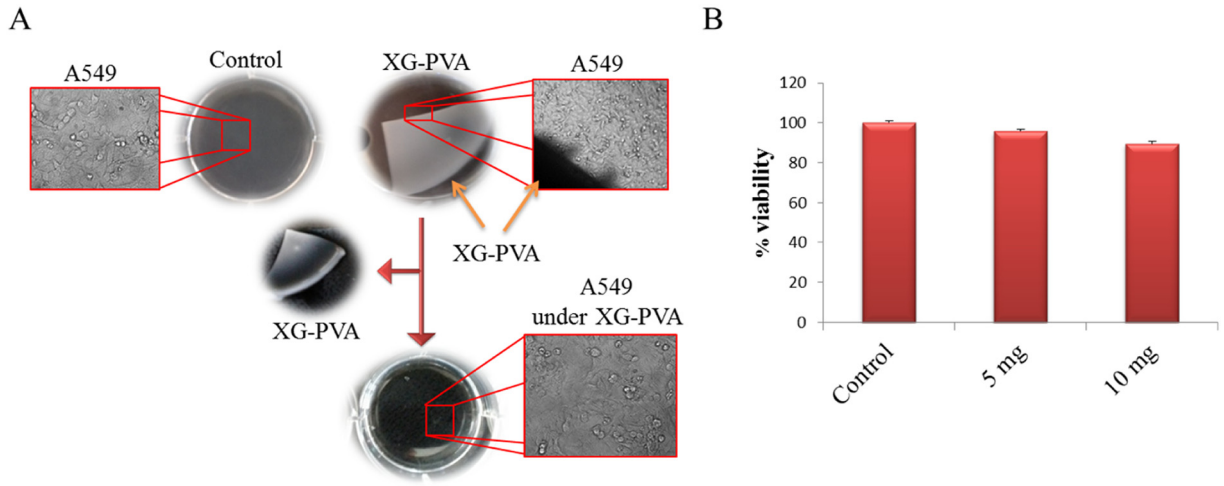

Fig. 3. XG-PVA film does not induce cellular toxicity. A) Representative morphological images of cells incubated or not (Control) adjacent and under the film. B) MTS assay of cells incubated or not (Control) with XG-PVA film with different weights (5 and 10 mg) for 48 h.

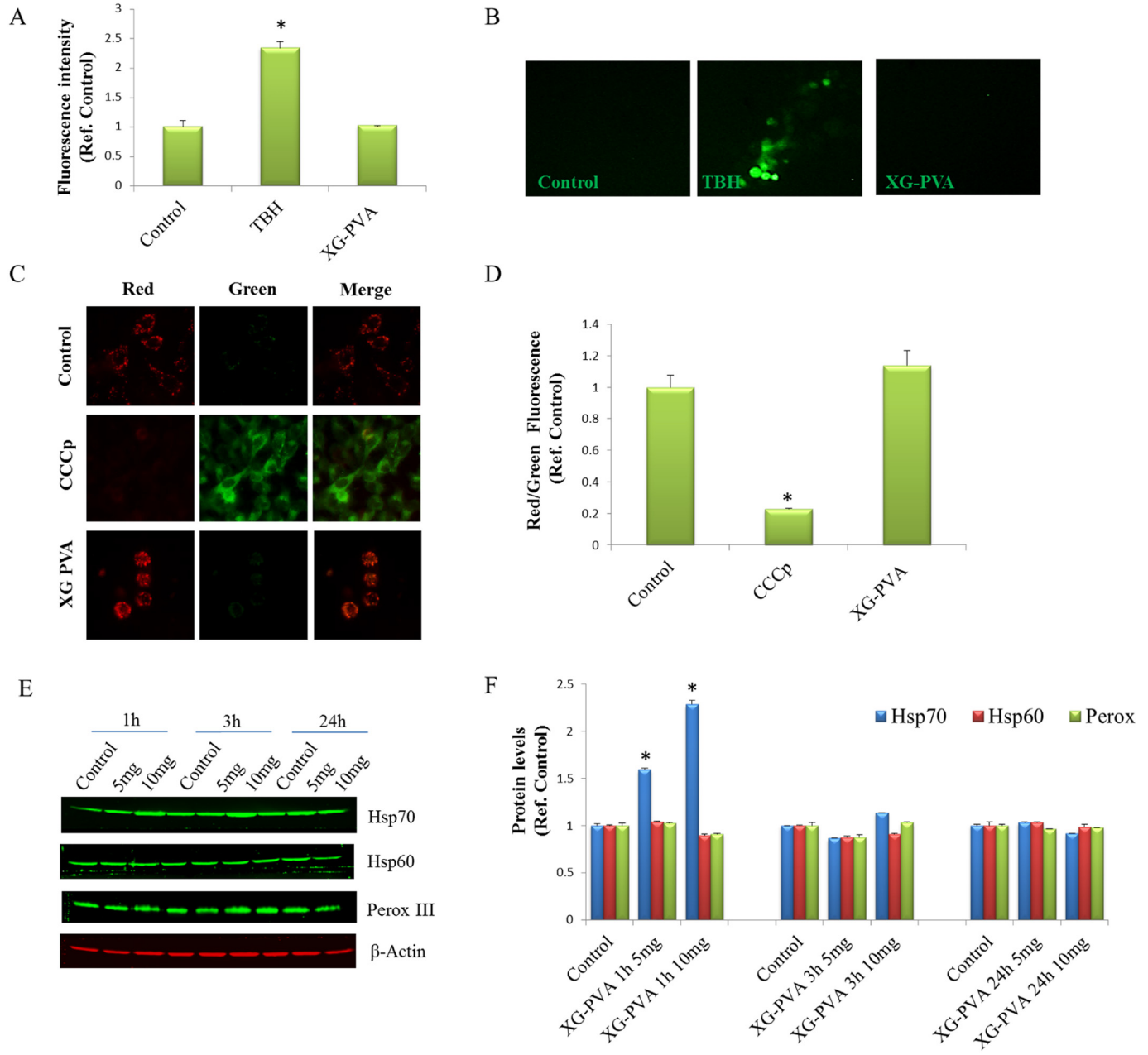

Fig. 4. XG-PVA film does not activate oxidative stress and mitochondrial dysfunction in A549 cells. A) DCF assay of A549 cells incubated or not (Control) with XG-PV film or with TBH, as positive control. B) Representative microscopic images of DCF assay. C) Representative fluorescent images of untreated cells (Control) or treated with XG-PVA film or with CCCp, as positive control and submitted to JC-1 assay. D) Histogram relative to the red/green fluorescence intensity ratio shown in C. E) Western blot of protein extracted from cells treated with different weights (5 and 10 mg) of XG-PVA and incubated with anti-Hsp70, anti-Hsp60 and anti-peroxiredoxin III (Perox III). Uniformity of gel loading was confirmed with β-actin used as a standard. F) Quantification of immunoreactivity performed by densitometric analysis. *$p < 0.05$ *vs.* control.

organized intracellular actin network, supporting the existence of an adhesion process. Thus, XG-PVA film showed a partial attachment, and confirmed its ability to support cell viability and growth.

3.6. XG-PVA film hemocompatibility

Erythrocytes wellness or destruction is a hemocompatibility index. Blood was incubated with XG-PVA film for 3 h and the number of erythrocytes and their parameters were measured. As shown in Fig. 6A and B, no significant difference in all the analyzed parameters was evidenced with respect to the control. Furthermore, hemolysis ratio was analyzed by using a spectrophotometrical test, which measures the amount of free plasma hemoglobin (Hb). In Fig. 6C is evidenced that the hemolysis percentage induced by the presence of the XG-PVA film in the blood sample was comparable to the untreated control, whereas whole hemolysis was observable in the sample treated with Triton-X, used as positive control. The result was supported by erythrocyte microscopic analysis (Fig. 6C).

3.7. XG-PVA film hemostatic effects

To ascertain that the dressing material did not induce platelet activation and consequently thrombus formation, different parameters were measured (ISO10993-4). Blood was placed in contact with the film for 3 h. Platelets indices (PI), such as number, mean volume (MPV), distribution width (PDW) and plateletcrit (PCT) were in the human standard range, indicating that no activation occurred (Table 1). Since the coagulation cascade, including intrinsic and extrinsic pathways, leads to

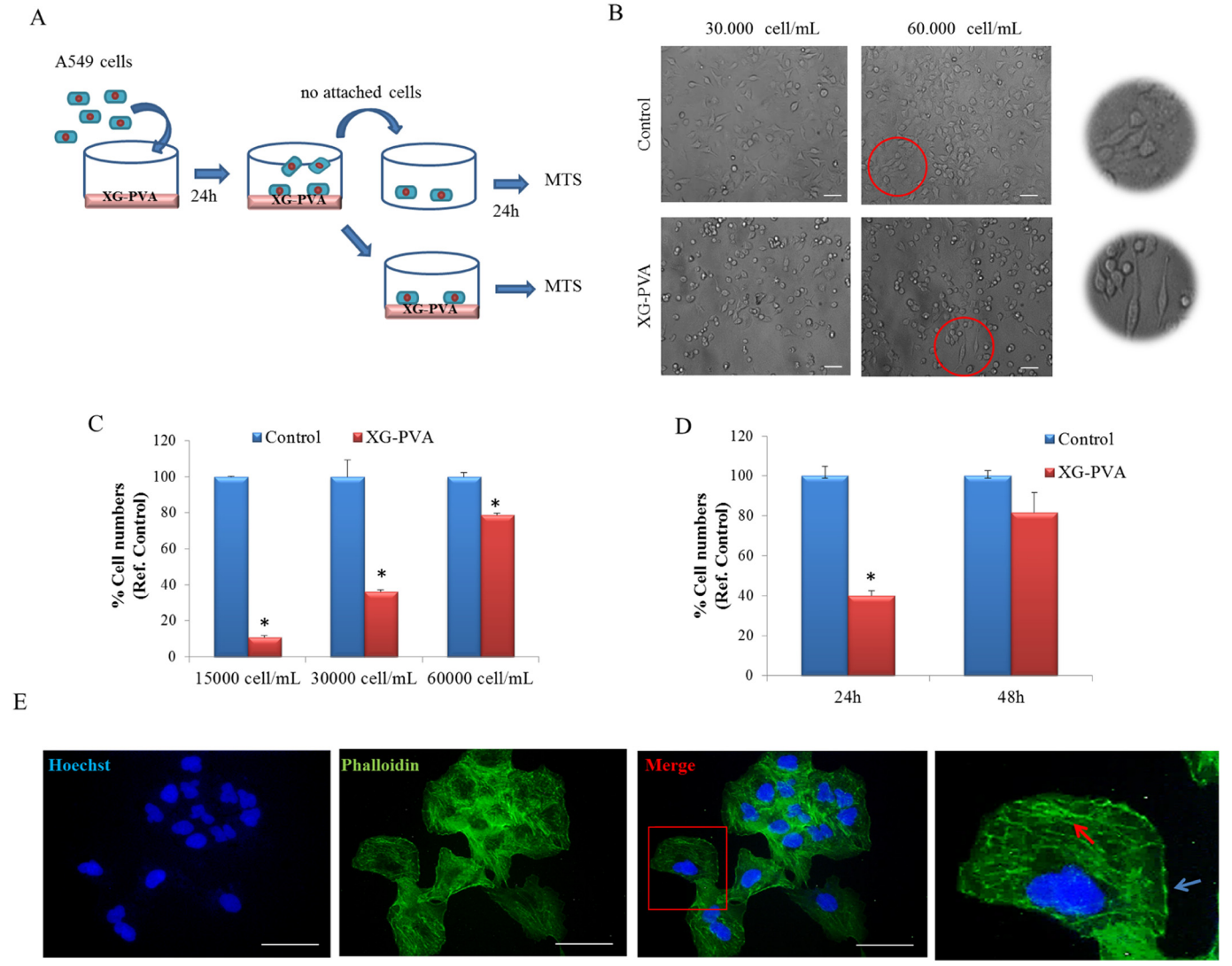

Fig. 5. A549 cells partially adhere on the XG-PVA film. A) Experimental scheme of cell attachment assay; B) Morphology of cells adhered on CCP (Control) and on XG-PVA film at various cell densities. C) MTS assay of the adhered cells on XG-PVA film, relatively to the control, seeded at various cell densities. D) MTS assay of non-adherent cells on the XG-PVA film, relatively to the control, seeded at different cell density. E) MTS assay at 24 and 48 h of attached living cells, relatively to the control. F) Immunofluorescence of cells stained with phalloidin and Hoechst 3342. Blue arrow indicates the focal adhesion and the red arrow indicates the intracellular actin network. Bar 50 μm. *p < 0.05 *vs.* control.

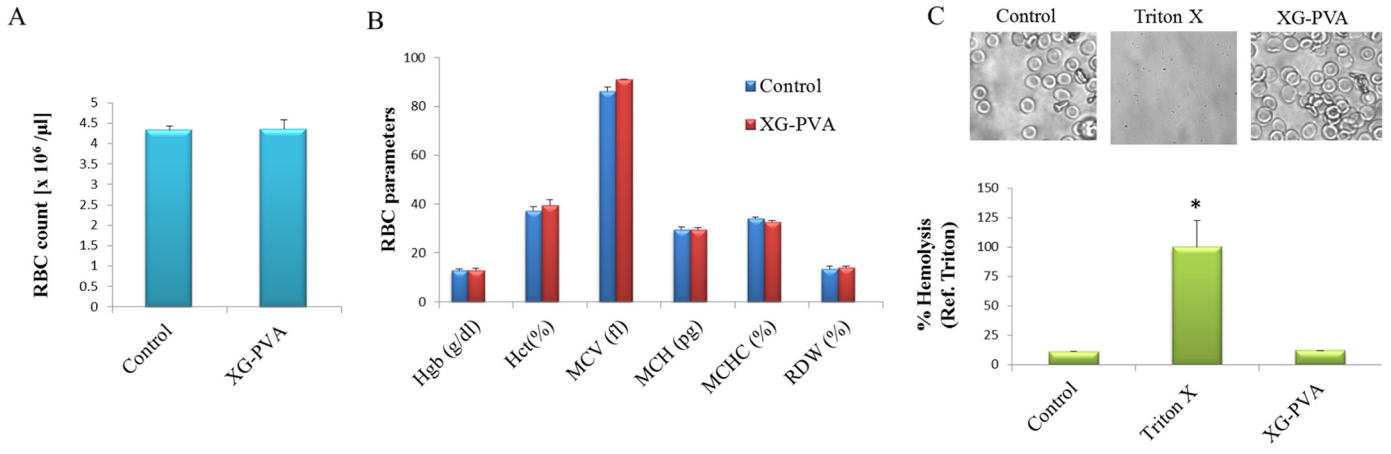

Fig. 6. XG-PVA film does not induce erythrocytes alteration and hemolytic response. Blood from human volunteer donors was incubated or not (Control) with XG-PVA film. A) Red blood cell (RBC) count. B) RBC parameters (Hgb = hemoglobin, Hct = hematocrit, MCV = Mean Corpuscular Volume, MCH = Mean Corpuscular Hemoglobin, MCHC = Mean Corpuscular Hemoglobin Concentration, RDW = Red Cell Distribution Width). C) Histogram and microscopic images of hemolysis assay of erythrocytes (Control) alone or incubated with Triton-X, as positive control, or with XG-PVA film. *p < 0.05 *vs.* control.

Table 1
XG-PVA film does not alter platelet parameters. Blood from human volunteer donors was incubated or not (Control) with XG-PVA film. Platelet count and platelet indices including: mean platelet volume (MPV), plateletcrit (PCT) and platelet distribution width (PDW). C) Prothrombin time (PT).

	Platelet count [$\times 10^3$ μL]	MPV (fl)	PCT (%)	PDW (%)
Control	353.5 ± 37.5	11.8 ± 3,9	0.263 ± 0.11	16.4 ± 2.26
XG-PVA	318.5 ± 61.5	11.7 ± 0,9	0.247 ± 0.21	16.7 ± 3.18

thrombin activation and fibrinogen to fibrin conversion [39], additional parameters were assessed. Index of coagulation disorders, such as prothrombin time (PT) and activated partial thromboplastin time (aPTT), were analyzed and the values were in the human standard range (Table 2). In order to complete the coagulation framework, the antithrombin-III (aTIII) and plasma fibrinogen (PF) concentrations were measured and the results indicated that the value obtained in presence of XG-PVA film were comparable to the control (Table 2).

3.8. XG-PVA film immunogenicity

Potential activation of immunogenic response by XG-PVA film was tested by using blood samples. No statistically significant difference was found in the number and composition of the White Blood Cells (WBC) population with respect to the control (Fig. 7A, B). Moreover, since contact of blood with pathological agents or foreign materials could activate the complement pathway as a body defense reaction, the level of C3 and C4 in plasma was measured. No relevant modification of C3 and C4 concentration was detected in the samples incubated with XG-PVA film (Fig. 7C, D). Furthermore, we assessed the effect of XG-PVA film on inflammatory response, by using *in vitro* isolated human lymphocytes. Peripheral blood mononuclear cells (PBMCs) were incubated with samples of XG-PVA film or stimulated with either lipopolysaccharide (LPS) or H_2O_2, as activators of inflammatory response and cell stress respectively, and then subjected to MTS assay. The results shown in Fig. 7E and F indicated that, in the presence of XG-PVA samples, cell viability was comparable to the control (PBMC without XG-PVA film). In contrast, the cells incubated with LPS were redoubled and when incubated with H_2O_2 were reduced to 50%. The corresponding morphological images are showed in Fig. 7F. All together, these data indicated that the hydrogel film did not activate, *in vitro,* neither immune response or cellular stress, thus supporting the suitability of XG-PVA material for wound healing applications.

3.9. Effect of XG-PVA film on bacterial growth

Nonpathogenic *E. coli* bacteria were used to investigate the behavior of XG-PVA film when in contact with bacteria. Aliquots of the o.n. bacteria growth were incubated in two test tubes containing LB for 120 min. Hence, a film sample was added to one of the two test tubes (Fig. 8A). The bacterial growth was monitored spectrophotometrically for 240 min. No difference in the growth curves for the two test tubes was detected, indicating that the film did not inhibit bacterial growth (Fig. 8A). Moreover, *E. coli* were seeded on a LB agar plate and, after placing XG-PVA film on its surface, were o.n. incubated. In agreement with the above results, bacterial growth was not inhibited (Fig. 8B).

Table 2
XG-PVA film does not activate thrombogenic response. Prothrombin time (PT), activated partial thromboplastin time (aPTT), antithrombin-III (aTIII) concentration, plasma fibrinogen (PF) concentration.

	PT (sec)	aPTT (sec)	aTIII (mg/dL)	PF (mg/dL)
Control	12.7 ± 0.5	34.3 ± 3.5	25.9 ± 0.21	298.5 ± 16.26
XG-PVA	12 ± 0.4	35.5 ± 2.1	26.8 ± 0.28	315 ± 30.1

We tested the ability of the film to provide protection against bacterial infiltration. To this aim, XG-PVA film was placed on a LB agar plate and of *E. coli* were gently dropped in the center of the surface of the film. After 24 h, the agar below the film, the agar with bacteria without film, and agar far from the film were cut and incubated in LB medium and the bacterial growth was measured every 30 min (see Supporting Information fig. S1). The proliferation curves, shown in Fig. 8C, clearly indicated that XG-PVA film was able to prevent bacteria infiltration.

Bacterial retentivity was also investigated. *E. coli* were seeded on a LB agar plate and, after placing XG-PVA film on its surface, were o.n. incubated (see Supporting Information Fig. S1). The experimental results (Fig. 8D) indicated that the number of bacteria was significantly higher in the sample containing the film than in the one with the agar underneath the film, indicating that the wound dressing ha bacteria retention properties. Moreover, with the aim to provide antibacterial properties, different amounts of ampicillin were loaded on the film. The samples were placed on LB agar plates in which *E.coli* was plated (Fig. 8E). After 24 h of growth, an inhibition growth zone increasing in a dose dependent manner was formed, indicating that XG-PVA film can absorb and released the antibiotic (Fig. 8F).

4. Discussion

Crosslinked XG/PVA hydrogel film was prepared starting from XG and PVA solutions [21]. Chemical crosslinking was achieved using glutaraldehyde (GA) as crosslinking agent, yielding high gel fractions (*ca.* 93%). GA promotes the formation of acetal and hemiacetal bonds between XG chains, and between XG and PVA. Glycerol was added to the formulation before drying and provided the film with the desired flexibility and water retention properties. GA continues to react also during the drying process and promotes grafting of part of the glycerol to the polymeric network. The resulting film is homogeneous, slightly opaque, easy to handle, flexible and conformable (see Fig. S2). It is able to absorb large amounts of aqueous fluids. In particular, the equilibrium swelling degree in PBS was about 350% of the initial weight.

The hydrolytic degradation of this film was investigated over five weeks. The non-grafted glycerol was rapidly released within the first hours of incubation. The erosion of the polymeric network occurred more rapidly during the first week, accounting for about 50% of mass loss in the first 4 days, then slowly continued in the following weeks, without reaching a plateau within the investigated time window. The observed slight FTIR spectral change can be the result of cleavage of grafted-GA (disappearance of the aldehyde terminal group) and restoration of the characteristic t-OH of the polysaccharide. Significant changes in the morphology of the "degraded" film were observed already after 24 h (see Fig. 1B). The as-prepared film showed larger cavities of irregular shape with internal septa. The "degraded film" had significant larger pores with thicker walls, which were in agreement with the observed weight loss and also suggested a reorganisation of the polymeric network, probably driven by XG self-assembly. A strong time-dependence of the morphology of the as-prepared films and similar changes in pores structure upon hydrolytic degradation were also observed in partially degalactosylated XG physical gels [40]. We have already demonstrated that the leaching components from the film, released over two weeks, do not cause cytotoxic effects on cultured cells [21].

The biological safety of the film was investigated by both direct-contact and MTS methods according to ISO 10993-5 standard protocols. In both adjacent and contact areas of XG-PVA film with cells, the cell morphology was unaltered as occurs for other biomaterials [41,42]. Similarly, after film removal, the underlying cell layer appeared unaffected and absence of cytotoxicity was supported by 90% viability. These data confirmed that during the cell-film contact time no toxic components were released, in good agreement with our previous results [21].

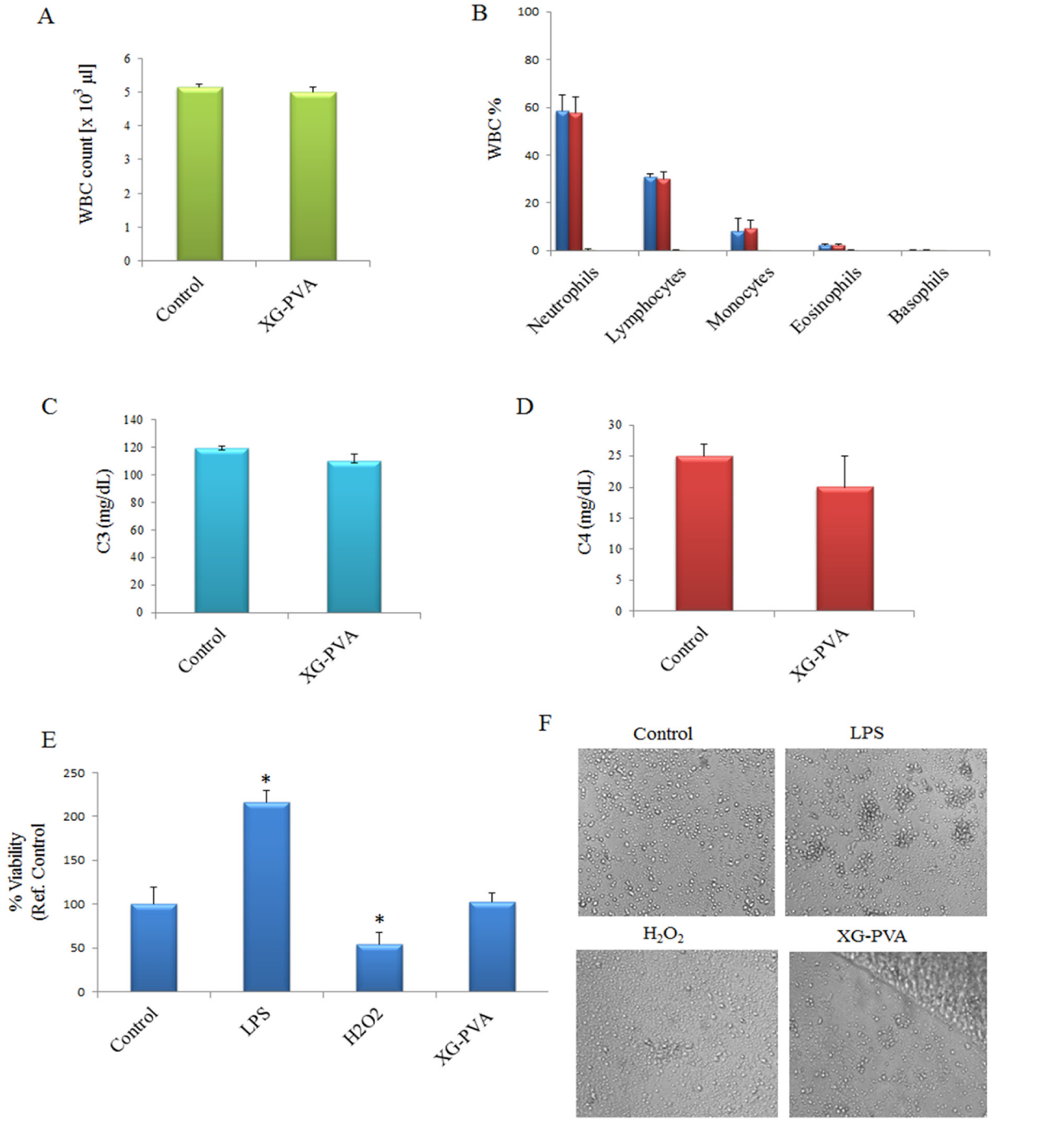

Fig. 7. XG-PVA film does not activate immunogenic response. White blood cells (WBC) were incubated or not (Control) with XG-PVA film. A) WBC count. B) Composition of the WBC population. C3 (C) and C4 (D) plasma concentrations. E) Percentage of viability of PBMCs incubated or not (Control) with LPS, H_2O_2 and XG-PVA film, and submitted to MTS assay. F) Microscopic images of PBMCs incubated or not (Control) with LPS, H_2O_2 and XG-PVA film. *$p < 0.05$ *vs.* control.

Biocompatibility was also tested by evaluating other injurious mechanisms that a biomaterial could activate when in contact with a biological environment, such as oxidative stress, mitochondrial dysfunction and apoptosis. All these mechanisms, if activated, can delay or prevent wound healing. Detection of ROS in response to a biomaterial is considered a method to evaluate the host reaction [34]. Both *in vitro* and *in vivo* experiments have, indeed, demonstrated that biomaterials can differently modulate oxidative stress [43,44]. Furthermore, we analyzed Hsp70, Hsp60 and peroxiredoxin III stress protein expressions as markers of cell-polymer interaction response. On the basis of the Hsp70 modulation, we can hypothesize that the contact with the foreign material has stimulated a cell defense or adaptive response, but in a short time cellular homeostasis was re-established, avoiding cell degeneration.

Cell adhesiveness is not a common feature of conventional hydrogel dressings [13], but in the prospect of developing active dressings that contribute to tissue regeneration, some degree of cell adhesiveness can be a desired property [45]. Indeed, XG-PVA film showed partial cell adhesiveness and supported cell growth, as demonstrated by the attachment assays. As visualized by optical and fluorescence microscopies, cells in contact to the film showed their normal shape. Cell attachment is also supported by both the presence of focal adhesions between cells and substrate and an organized intracellular actin network, indicating nascent adhesion points [46]. These data are also

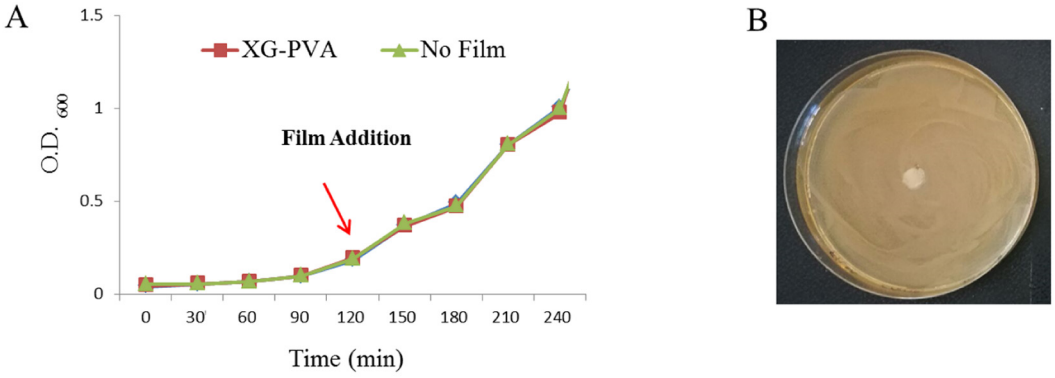

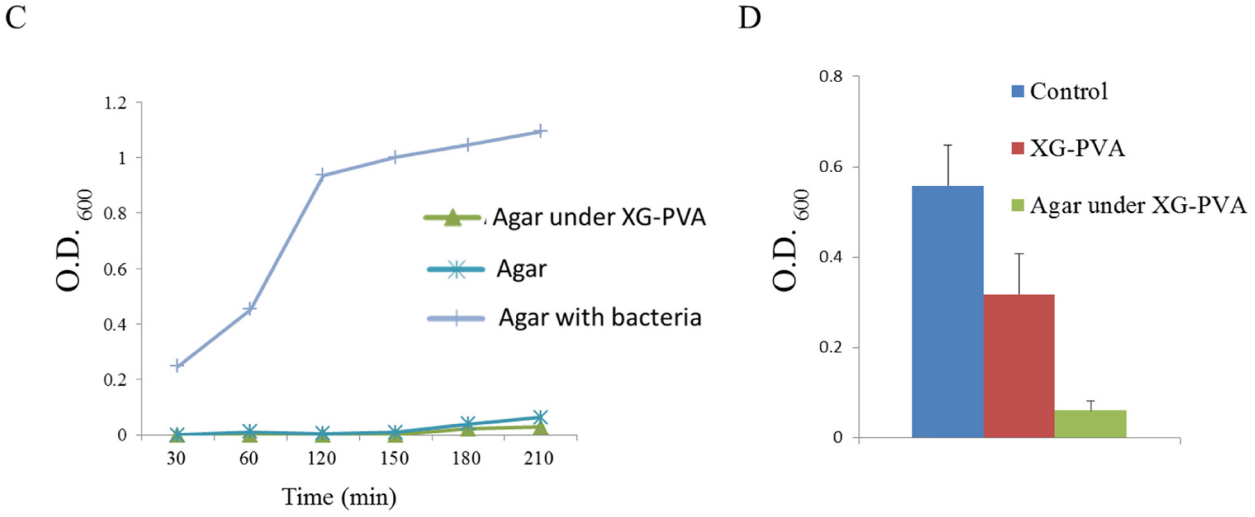

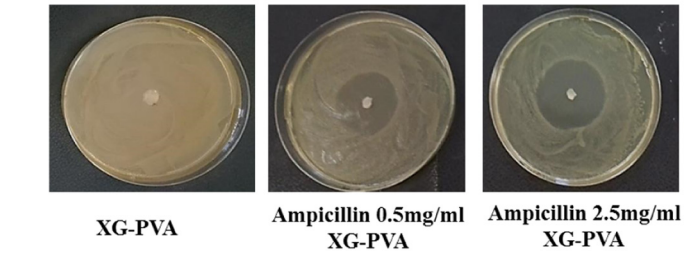

F

Sample	Inhibition zone
XG-PVA	N.D.
Ampicillin 0.5mg/ml XG-PVA	2,9 cm
Ampicillin 2.5mg/ml XG-PVA	4 cm

Fig. 8. XG-PVA film shows antimicrobial properties and ability to adsorb and release antibiotic. A) Bacteria were growth in LB medium and after 120 min XG-PVA film was added or not (Control) and optical density ($O.D._{600}$) measured every 30 min. B) Bacteria growth in LB plate in presence of XG-PVA film. C) For the infiltration test pieces of agar with bacteria, agar control (Agar) and agar under the film were incubate in LB medium and $O.D._{600}$ was measured at different times. D) For the retentivity test bacteria growth in XG-PVA film (XG-PVA), in the portion of LB agar under the film (Agar under XG-PVA) and in a portion of the LB agar far from the film (Control), were incubated in LB medium and $O.D._{600}$ were measured after 120 min. E) XG-PVA film soaked or not with ampicillin was plated on LB plate. Photograph shows the effect of ampicillin at two concentrations (0.5 mg/mL and 2.5 mg/mL) on *E. coli* colonies. The Table (F) indicates the measure of the inhibition zone diameter (N.D. = not detected).

backed up by the film ability to adsorb serum proteins (see figures Ref [47]), probably due to its amphiphilic nature and suitable pore size [48]. In a previous work of some of the Authors, a strong affinity between a growth factor and a partially degalactosylated variant of XG was observed [17]. In the present context, we can argue that the absorbed serum proteins could mediate cellular attachment to the film [49].

An ideal dressing should require an appropriate level of adhesion to the wound bed, which guarantees attachment to the skin as well as painless removal. Recently, the term 'atraumatic dressings' has been adopted to describe both adhesive and non-adhesive dressings that can be removed without trauma [50]. When our film is removed from the cell monolayer, it does not cause damage or exfoliation, thus suggesting that cell-cell adhesion was stronger than cell-biomaterial interaction. When in contact with the cells, and often also due to cell *sec*reted molecules, hydrogels modify their morphology and surface wettability, hence their mechanical and (bio)functional properties. This introduces a fourth dimension to their 3D structure [51]. The morphology of our film was indeed changing over time when exposed to the swelling medium, which could support a change of cellular adhesiveness.

Blood is the first tissue coming in contact with a wound dressing material and, depending on its components, adverse health effects can occur [52]. For this reason, *in vitro* hemocompatibility is one of the biological evaluations recommended by ISO 10993-4 guidelines for the

validation of medical devices. The characterizations performed to investigate XG-PVA film-blood interactions, such as hemolysis and thrombogenicity, leucocytes and complement activation supported its hemocompatibility. As reported, when a dressing material interacts with blood plasma, proteins and platelets, could be adsorbed to its surface and this could induce thrombotic events [53]. The dressing material here presented did not activate coagulation or fibrinolysis, probably thanks to its partial adhesiveness and non-ionic molecular structure. Hence, even if supplementary tests can be performed, on the basis of the present results we can consider XG-PVA film hemocompatible.

XG-PVA film did not appear to interfere with the blood defense systems, maintaining the white blood cells number and percentage of each type in the healthy range. Immunogenicity absence was also supported by the experiment in which human PBMCs treated with XG-PVA were not affected. Furthermore, it has been reported that complement activation upon contact with biomaterial depends on the material surface composition [54,55]. The measurement of C3 and C4 levels, biomarkers of complement activation, supported that the dressing material did not activate immune response.

Bacterial wound infection is one of the causes that prevents the healing process and leads to serious complications, such as septicemia [56–58]. XG-PVA film has not intrinsic antibacterial properties, but shows bacterial retentivity, *i.e.* the potency to entrap bacteria and prevent them leaking out. This feature could be due to the porous microstructure and the chemical composition of the XG-PVA film. In addition, XG-PVA film inhibited bacterial infiltration indicating that the film can act as a barrier against bacteria, which is a required propriety for an ideal wound dressing. Since antimicrobial agents have the ability of preventing and defeating the insurgence of infections, ampicillin was loaded on the dressing film to provide antimicrobial activity. Antibiotic inhibited bacterial growth indicating that the XG-PVA film released it and its activity was maintained. The ability to adsorb and release active molecules, as also demonstrated with the Atto 633 fluorescent probe, can be favorably exploited for the development of medicated wound dressing variants. Interestingly, the same film has been also integrated with a powerless sensing and communication platform for remote monitoring, therefore in its further development will be able to acquire information on relevant biological parameters and provide support for remote monitoring of the wound healing itself [59,60].

5. Conclusions

This work mainly addresses the relationships between physicochemical and morphological properties of a purposely-engineered XG-PVA film and its *in vitro* biological behavior for wound healing applications. The film is homogeneous, slightly opaque, easy to handle, flexible, conformable and shows partial cell adhesiveness, thus suggesting that it can provide protection to the wound but at the same time be removed without pain or trauma, probably due the observed morphological rearrangements upon degradation. XG-PVA is also able to retain aqueous fluids and absorb proteins, suggesting that it can grant a moist wound environment while absorbing exudates.

We demonstrated that XG-PVA film is fully cyto-compatible, blood-compatible and does not activate any immunogenic response; therefore, we expect it to be biological safe when in contact with the wound. XG-PVA film inhibits *E. coli* infiltration, which supports its protective function against bacterial infection, and bacterial retentivity, properties that are very important for wound dressing. We believe that all the results here collected encourage in proceeding with the *in vivo* evaluation of the XG-PVA film as wound dressing materials.

Acknowledgments

We gratefully acknowledge DSP Gokyo, Food and Chemical Co., Japan, and particularly Dr. K. Yamatoya, Ms. M. Shirakawa, Dr. A. Tabuchi for supplying the xyloglucan sample. Furthermore, the authors thank Mr. Luca Caruana IBIM-CNR, Mr. Fulvio Ferrante, Dr. Alessia Provenzano (IBF-CNR) and Dr. Paolo Guerra (DIID-UniPA) for useful technical support. The research was partially supported by the Italian Ministry of University and Research in the framework of the Flagship Project NanoMAX (no B79E13000270005).

Appendix A. Supplementary data

Supplementary data to this article can be found online at https://doi.org/10.1016/j.ijbiomac.2018.10.078.

References

[1] M.C. Robson, D.L. Steed, M.G. Franz, Wound healing: biologic features and approaches to maximize healing trajectories, Curr. Probl. Surg. 38 (2001) 72–140.
[2] G.C. Gurtner, S. Werner, Y. Barrandon, M.T. Longaker, Wound repair and regeneration, Nature 453 (2008) 314–321.
[3] S. Dhivya, V.V. Padma, E. Santhini, Wound dressings - a review, Biomedicine 5 (2015) 24–28.
[4] F.A. Toppo, R.S. Pawar, Novel drug delivery strategies and approaches for wound healing managements, J. Crit. Rev. 2 (2015) 12–20.
[5] J.S. Boateng, K.H. Matthews, H.N. Stevens, G.M. Eccleston, Wound healing dressings and drug delivery systems: a review, J. Pharm. Sci. 97 (2008) 2892–2923.
[6] G.D. Mogoşanu, A.M. Grumezescu, Natural and synthetic polymers for wounds and burns dressing, Int. J. Pharm. 25 (2014) 127–136.
[7] M. Norouzi, S.M. Boroujeni, N. Omidvarkordshouli, M. Soleimani, Advances in skin regeneration: application of electrospun scaffolds, Adv. Healthc. Mater. 4 (2015) 1114–1133.
[8] M. Ishihara, K. Nakanishi, K. Ono, M. Sato, M. Kikuchi, Y. Saito, H. Yura, T. Matsui, H. Hattori, M. Uenoyama, A. Kurita, Photocrosslinkable chitosan as a dressing for wound occlusion and accelerator in healing process, Biomaterials 23 (2002) 833–840.
[9] C. Alemdaroglu, Z. Değim, N. Celebi, F. Zor, S. Oztürk, D. Erdoğan, An investigation on burn wound healing in rats with chitosan gel formulation containing epidermal growth factor, Burns 32 (2006) 319–327.
[10] I. Liakos, L. Rizzello, D.J. Scurr, P.P. Pompa, I. Bayer, A. Athanassiou, All-natural composite wound dressing films of essential oils encapsulated in sodium alginate with antimicrobial properties, Int. J. Pharm. 46 (2014) 137–145.
[11] M. Contardi, J.A. Heredia-Guerrero, G. Perotto, P. Valentini, P.P. Pompa, R. Spanò, L. Goldoni, R. Bertorelli, A. Athanassiou, I.S. Bayer, Transparent ciprofloxacin-povidone antibiotic films and nanofiber mats as potential skin and wound care dressings, Eur. J. Pharm. Sci. 104 (2017) 133–144.
[12] E.A. Kamoun, E.S. Kenawy, X. Chen, A review on polymeric hydrogel membranes for wound dressing applications: PVA-based hydrogel dressings, J. Adv. Res. 8 (2017) 217–233.
[13] M. Madaghiele, C. Demitri, A. Sannino, L. Ambrosio, Polymeric hydrogels for burn wound care: advanced skin wound dressings and regenerative templates, Burns & Trauma 2 (2014) 153–161.
[14] C.J. Beukelman, A.J. van den Berg, M.J. Hoekstra, R. Uhl, K. Reimer, S. Mueller, Anti-inflammatory properties of a liposomal hydrogel with povidone-iodine (Repithel) for wound healing in vitro, Burns 34 (2008) 845–855.
[15] L.C. Hsu, B.Y. Peng, M.S. Chen, B. Thalib, M. Ruslin, T.D.X. Tung, H.H. Chou, K.L. Ou, The potential of the stem cells composite hydrogel wound dressings for promoting wound healing and skin regeneration: in vitro and in vivo evaluation, J. Biomed. Mater. Res. B Appl. Biomater. 26 (2018) (z`2018:00B:000–000).
[16] He Liu, Chenyu Wang, Chen Li, Yanguo Qin, Zhonghan Wang, Fan Yang, Zuhao Li, Jincheng Wang, A functional chitosan-based hydrogel as a wound dressing and drug delivery system in the treatment of wound healing, RSC Adv. 8 (2018) 7533–7549.
[17] C. Dispenza, S. Todaro, D. Bulone, M.A. Sabatino, G. Ghersi, P.L. San Biagio, C. Lo Presti, Physico-chemical and mechanical characterization of in-situ forming xyloglucan gels incorporating a growth factor to promote cartilage reconstruction, Mater. Sci. Eng. C Mater. Biol. Appl. 1 (2017) 745–752.
[18] M.C. Koetting, J.T. Peters, S.D. Steichen, N.A. Peppas, Stimulus-responsive hydrogels: theory, modern advances, and applicationns, Mater. Sci. Eng. R. Rep. 93 (2015) 1–49.
[19] F.J. O'Brien, B.A. Harley, I.V. Yannas, L.J. Gibson, The effect of pore size on cell adhesion in collagen-GAG scaffolds, Biomaterials 26 (2005) 433–441.
[20] L.T. Allen, M. Tosetto, I.S. Miller, D.P. O'Connor, S.C. Penney, I. Lynch, A.K. Keenan, S.R. Pennington, K.A. Dawson, W.M. Gallagher, Surface-induced changes in protein adsorption and implications for cellular phenotypic responses to surface interaction, Biomaterials 27 (2006) 3096–3108.
[21] A. Ajovalasit, M.A. Sabatino, S. Todaro, S. Alessi, D. Giacomazza, P. Picone, M. Di Carlo, C. Dispenza, Xyloglucan-based hydrogel films for wound dressing: structure-property relationships, Carbohydr. Polym. 1 (2018) 262–272.
[22] N.B. Shankaracharya, Tamarind-chemistry, technology and uses a critical appraisal, J. Food Sci. Technol. 35 (1998) 193–208.
[23] A. Mishra, A.V. Malhotra, Tamarind xyloglucan: a polysaccharide with versatile application potential, J. Mater. Chem. 19 (2009) 8528–8536.
[24] A. Semenzato, A. Costantini, G. Baratto, Green polymers in personal care products: rheological properties of tamarind seed polysaccharide, Cosmetics 2 (2014) 1–10.

[25] Y. Yuguchi, T. Fujiwara, H. Miwa, M. Shirakawa, H. Yajima, Color formation and gelation of xyloglucan upon addition of iodine solutions, Macromol. Rapid Commun. 26 (2005) 1315–1319.
[26] A. Giori, S. Arpini, S. Togni, Tamarind seed polysaccharide for use in the treatment of inflammatory diseases, EU patent WO2011147768 A1. (2011) December 1st.
[27] M.Y. Bin Mohamad, H.B. Akram, D.N. Bero, M.T. Rahman, Tamarind seed extract enhances epidermal wound healing, Int. J. Biol. 4 (2012) 81–88.
[28] W. Nie, A.M. Deters, Tamarind seed xyloglucans promote proliferation and migration of human skin cells through internalization via stimulation of proliferative signal transduction pathways, Dermatol. Res. Pract. (2013) 1–14.
[29] P. Lang, G. Masci, M. Dentini, V. Crescenzi, D. Cooke, J. Gidley, C. Fanutti, J.S.G. Reid, Tamarind seed polysaccharide: preparation, characterisation and solution properties of carboxylated, sulphated and alkylaminated derivatives, Carbohydr. Polym. 17 (1992) 185–198.
[30] A.D. Kulkarni, A.A. Joshi, C.L. Patil, P.D. Amale, H.M. Patel, S.J. Surana, V.S. Belgamwar, K.S. Chaudhari, C.V. Pardeshi, Xyloglucan: a functional biomacromolecule for drug delivery applications, Int. J. Biol. Macromol. 104 ((2017) 799–812.
[31] S.N. Eğe, in: Houghton Mifflin (Ed.), Organic Chemistry: Structure and Reactivity, 1999 , (ISBN 10: 0395902231/ISBN 13: 9780395902233).
[32] P. Picone, G. Navarra, C. Peres, M. Contardi, P.L. San Biagio, M. Di Carlo, D. Giacomazza, V. Militello, Data Concerning the Proteolytic Resistance and Oxidative Stress in LAN5 Cells After Treatment With BSA Hydrogels, Data Brief 6, 2016 324–327.
[33] P. Picone, L.A. Ditta, M.A. Sabatino, V. Militello, P.L. San Biagio, M.L. Di Giacinto, L. Cristaldi, D. Nuzzo, C. Dispenza, D. Giacomazza, M. Di Carlo, Ionizing radiation engineered nanogels as insulin nanocarriers for the development of a new strategy for the treatment of Alzheimer's disease, Biomaterials 80 (2016) 179–194.
[34] A. Bruininck, R. Luginbuehl, Evaluation of biocompatibility using in vitro methods: interpretation and limitations, Adv. Biochem. Eng. Biotechnol. 126 (2012) 117–152.
[35] S. Kato, T. Akagi, K. Sugimura, A. Kishida, M. Akashi, Evaluation of biological responses to polymeric biomaterials by RT-PCR analysis III: study of HSP 70, 90 and 47 mRNA expression, Biomaterials 19 (1998) 821–827.
[36] S. Hradilová, M. Havrdová, A. Panáček, L. Kvítek, R. Zbořil, Hsp70 as an indicator of stress in the cells after contact with nanoparticles, J. Phys. Conf. Ser. 617 (2015) 012023.
[37] S.C. Gupta, A. Sharma, M. Mishra, R.K. Mishra, D.K. Chowdhuri, Heat shock proteins in toxicology: how close and how far? Life Sci. 86 (2010) 377–384.
[38] T. Rabilloud, M. Heller, F. Gasnier, S. Luche, C. Rey, R. Aebersold, M. Benahmed, P. Louisot, J. Lunardi, Proteomics analysis of cellular response to oxidative stress. Evidence for in vivo overoxidation of peroxiredoxins at their active site, J. Biol. Chem. 31 (2002) 19396–19401.
[39] M.B. Gorbet, M.V. Sefton, Biomaterial-associated thrombosis: roles of coagulation factors, complement, platelets and leukocytes, Biomaterials 25 (2004) 5681–5703.
[40] S. Todaro, M.A. Sabatino, M.R. Mangione, P. Picone, M.L. Di Giacinto, D. Bulone, C. Dispenza, Temporal control of xyloglucan self-assembly into layered structures by radiation-induced degradation, Carbohydr. Polym. 5 (2016) 382–390.
[41] G. Navarra, C. Peres, M. Contardi, P. Picone, P.L. San Biagio, M. Di Carlo, D. Giacomazza, V. Militello, Heat- and pH-induced BSA conformational changes, hydrogel formation and application as 3D cell scaffold, Arch. Biochem. Biophys. 15 (2016) 134–142.
[42] P.S. Sundaran, A. Bhaskaran, S.T. Alex, T. Prasad, V.H. Haritha, Y. Anie, T.V. Kumary, P.R. Anil Kumar, Drug loaded microbeads entrapped electrospun mat for wound dressing application, J. Mater. Sci. Mater. Med. 28 (2017) 88.
[43] W.F. Liu, M. Ma, K.M. Bratlie, T.T. Dang, R. Langer, D.G. Anderson, Real-time in vivo detection of biomaterial-induced reactive oxygen species, Biomaterials 32 (2011) 1796–1801.
[44] R. Gharibi, H. Yeganeh, A. Rezapour-Lactoee, Z.M. Hassan, Stimulation of wound healing by electroactive, antibacterial, and antioxidant polyurethane/siloxane dressing membranes: in vitro and in vivo evaluations, ACS Appl. Mater. Interfaces 4 (2015) 24296–24311.
[45] C. Ghobril, M.W. Grinstaff, The chemistry and engineering of polymeric hydrogel adhesives for wound closure: a tutorial, Chem. Soc. Rev. (7) (2015) 1820–1835.
[46] C. Ciobanasu, B. Faivre, C. Le Clainche, Actin dynamics associated with focal adhesions, Int. J. Cell. Biol. 2012 (2012) 941292.
[47] P. Picone, M.A. Sabatino, A. Ajovalasit, O.R. Brancato, D. Giacomazza, C. Dispenza, M. Di Carlo, Data concerning the proteins absorption property of xyloglucan-based hydrogel films, Data Brief (2018) (submitted for publication).
[48] R.A. Perez, G. Mestres, Role of pore size and morphology in musculo-skeletal tissue regeneration, Mater. Sci. Eng. C Mater. Biol. Appl. 1 (2016) 922–939.
[49] C.J. Wilson, R.E. Clegg, D. Leavesley, M.J. Pearcy, Mediation of biomaterial-cell interactions by adsorbed proteins: a review, Tissue Eng. 11 (2005) 1–18.
[50] S. Thomas, Atraumatic Dressings. World Wide Wounds, Online January 2003. Available from URL: http://www.worldwidewounds.com/2003/january/Thomas/Atraumatic-Dressings.html, Accessed date: 4 May 2018.
[51] A.M. Hilderbrand, E.M. Ovadia, M.S. Rehmann, P.M. Kharkar, C. Guo, A.M. Kloxin, Biomaterials for 4D stem cell culture, Curr. Opin. Solid State Mater. Sci. 20 (2016) 212–224.
[52] M.S. Bakshi, Nanotoxicity in systemic circulation and wound healing, Chem. Res. Toxicol. 30 (2017) 1253–1274.
[53] L. Xu, J.W. Bauer, C.A. Siedlecki, Proteins, platelets, and blood coagulation at biomaterial interfaces, Colloids Surf. B Biointerfaces 124 (2014) 49–68.
[54] B. Nilsson, K.N. Ekdahl, T.E. Mollnes, J.D. Lambris, The role of complement in biomaterial-induced inflammation, Mol. Immunol. 44 (2007) 82–94.
[55] P. Tengvall, A. Askendal, I.I. Lundstrom, Ellipsometric in vitro studies on the activation of complement by human immunoglobulins M and G after adsorption to methylated silicon, Colloids Surf. B Biointerfaces 20 (2001) 51–62.
[56] R. Jayakumar, M. Prabaharan, P.T. Sudheesh Kumar, S.V. Nair, H. Tamura, Biomaterials based on chitin and chitosan in wound dressing applications, Biotechnol. Adv. (3) (2011) 322–337.
[57] P.T. Kumar, V.K. Lakshmanan, T.V. Anilkumar, C. Ramya, P. Reshmi, A.G. Unnikrishnan, S.V. Nair, R. Jayakumar, Flexible and microporous chitosan hydrogel/nano ZnO composite bandages for wound dressing: in vitro and in vivo evaluation, ACS Appl. Mater. Interfaces 4 (2012) 2618–2629.
[58] T. Fujiwara, K. Hosokawa, T. Kubo, Comparative study of antibacterial effects and bacterial retentivity of wound dressings, Eplasty 13 (2013) e5.
[59] C. Occhiuzzi, A. Ajovalasit, M.A. Sabatino, C. Dispenza, G. Marrocco, RFID epidermal sensor including hydrogel membranes for wound monitoring and healing, 2015 IEEE Int. Conf. RFID (RFID), ISBN: 978-1-4799-1937-6 2015, pp. 182–188, https://doi.org/10.1109/RFID.2015.7113090.
[60] A. Ajovalasit, M.C. Caccami, S. Amendola, M.A. Sabatino, G. Alotta, M. Zingales, D. Giacomazza, C. Occhiuzzi, G. Marrocco, C. Dispenza, Development and characterization of xyloglucan-poly(vinyl alcohol) hydrogel membrane for wireless smart wound dressings, Eur. Polym. J. 106 (2018) 214–222.